Analysis and Optimisation of Protein Alignment in Combined Electric and Magnetic Fields

Natalie-Rose Taylor[1], James Austerberry[1], Peter Laity[1], Gemma Newby[2], Paul Thompson[3], Oier Bikondoa[3] and Daniel Belton[1*]

1. Department of Chemical and Biological Sciences, University of Huddersfield, Queensgate, Huddersfield, HD1 3DH, UK
2. Diamond Light Source, Harwell Science and Innovation Campus, Didcot, Oxfordshire, OX11 0DE, UK
3. XMaS, The UK-CRG, European Synchrotron Radiation Facility, 6 Rue Jules Horowitz, BP 220, 38043 Grenoble, France
**Corresponding author. E-mail: d.j.belton@hud.ac.uk*

Introduction

The objective of this project is to completely align biological macromolecules in three dimensional space through the use of simultaneous electric and magnetic fields. Potential applications include improving protein crystallisation strategies and solving the structures of biological macromolecules without the need for crystals. Here we describe results from BM28 at ESRF.

Methods and Materials

Instrumentation

The XMaS beamline was used with a MAR165 CCD detector 94 cm away from the sample holder. The X-ray energy used was 11.5 keV, which equates to a wavelength of 0.108 nm. Overall, this gave a q-range of circa 0.05 to 0.4 $Å^{-1}$.

The electric field was applied using ADAS electronique ICV712 digital to analogue converter. The potential difference across the cell electrodes was monitored using a Keithley 2000 voltmeter and the current across the cell was monitored using a Keithley 286 picoammeter. The magnetic field was applied using the XMaS/AMI 4 Tesla superconducting magnet.

A bespoke plastic sample holder was made to accommodate two mica windows and two copper electrodes coated in gold, as shown in Figure 1. The overall sample holder was small enough to fit inside the 4 Tesla magnet and therefore allowed the application of simultaneous electric and magnetic fields, whilst being examined by X-ray scattering. The orientation of the electrodes could also be rotated in relation the direction of the magnetic field. Inlet and outlet tubes allowed the cell to be loaded with the liquid sample and subsequently emptied and flushed without dismantling the cell.

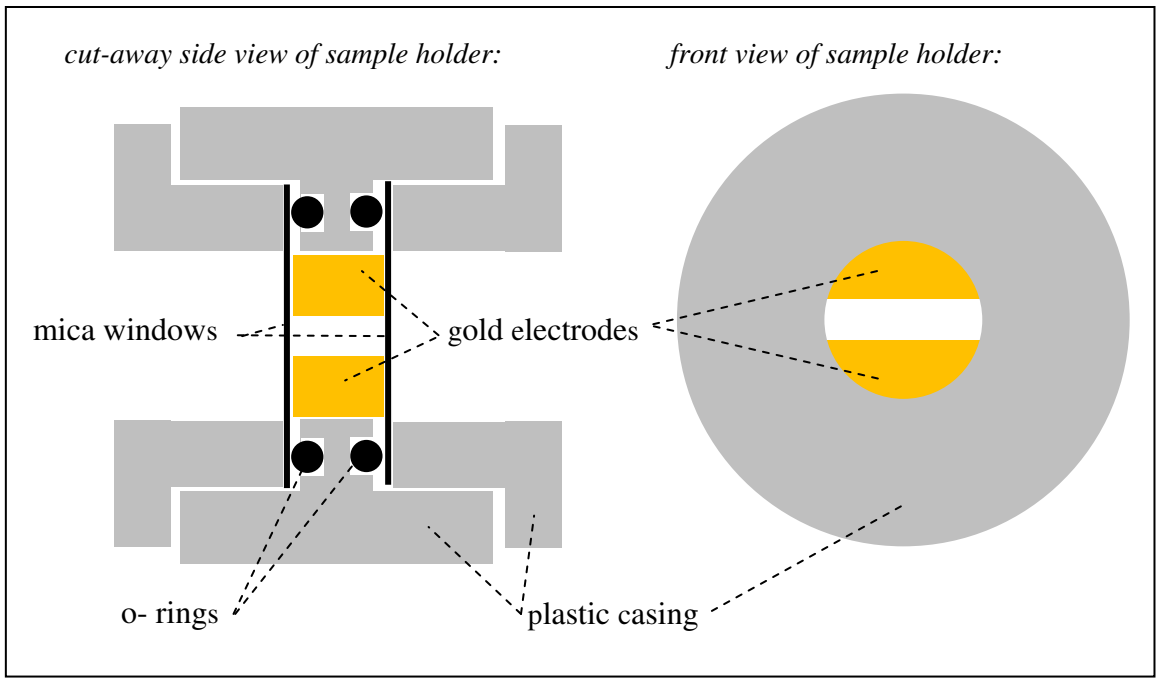

Figure 1. Bespoke sample holder for the application of simultaneous electric and magnetic fields

Sample Preparation

Glycerol and lysozyme were supplied by Sigma-Aldrich, UK. Glycerol purity was ≥99.5%. Lysozyme from chicken egg was supplied as lyophilized powder at a purity of ≥98%. 3g of glycerol was added to 3g of lysozyme lyophilized powder, followed by the gradual addition of high quality water up to 10ml, during this gradual addition the solution was sonicated and gently agitated at ambient temperature for 1h until the protein had dissolved.

Electric and Magnetic Fields

The magnetic field was applied by ramping the XMaS/AMI magnet from zero Tesla to 3.5 Tesla at 0.006 T/s, this was followed by a second ramp from 3.5 Tesla to the final field strength of 3.8 Tesla at 0.001 T/s. The sample was allowed to equilibrate under this field for one hour before the electric field was applied. The electric field was applied by ramping the ADAS digital to analogue converter from zero volts to 0.5 volts at 0.0125 V/s. The sample was allowed to equilibrate under both fields for a further ten minutes before any measurements were taken. The equilibration time used for single fields was one hour under the magnetic field or ten minutes under the electric field.

Measurements

The X-ray scattering patterns were recorded using a loop scan to collect twenty repeat scans with a 5 second exposure per scan and 1 minute between scans. The fast shutter was automatically closed between scans in order to minimise beam damage. The sample holder was flushed with a 4 M urea aqueous solution followed by high quality water between runs and fresh sample loaded. Care was taken to eliminate any bubbles from the sample chamber.

Results and Discussion

The 30% lysozyme in 30% glycerol solution was analysed under a range of different conditions in order to probe the effect of applying simultaneous electric and magnetic fields on sample behaviour and possible alignment. The different conditions included the application of no fields, electric field only, magnetic field only and simultaneous fields with different angles between the direction of the fields from 0° to 180°. The scattering pattern recorded under these different regimes is shown in Figure 2. When no fields are applied to the sample, the scattering pattern appears symmetrical and shows the presence of a ring that arises from the interference between the closely spaced protein molecules within the high concentration solution, see Figure 2a. When a single field is applied the scattering pattern appears unchanged and is again symmetrical, see Figure 2b and 2c. When both fields are applied simultaneously, the scattering pattern becomes asymmetric, see Figure 2d to 2h.

It is rather surprising to observe asymmetric scattering patterns, where the intensity is not the same either side of the beam centre. However, we have identified a structural model, consisting of highly oriented rods on a pseudo-lattice, which appears to explain the asymmetry (see Appendix 1). Indeed, this model would be consistent with the stated objective of the work, to achieve highly oriented macromolecules.

Figure 3 shows two sector integrations for 30% lysozyme in 30% glycerol solution under simultaneous electric and magnetic fields with 135° between fields. The first sector (lower left) covers the low intensity portion of the scattering, whilst the second sector (upper right) shows the high intensity portion of the scattering on the opposite side; both are shown in Figure 3a. The change in intensity versus q for these two sectors is shown in Figure 3b and this serves to further highlight the similarity between this experimental result and the theoretical scattering that arises from highly oriented molecules on a pseudo-lattice *cf.* Figure 7. Clearly, the combination of electric and magnetic fields induces a strong alignment of the proteins, in agreement with the theory outlined in Appendix 1. The full analysis of the data is ongoing. These results confirm that electric and magnetic fields can be used to align macromolecules and merits further investigation.

In future work, the small and wide angle scattering of further model systems will be measured to probe different length scales. The effect of temperature on samples will also be tested, which will require some modifications to the sample cell.

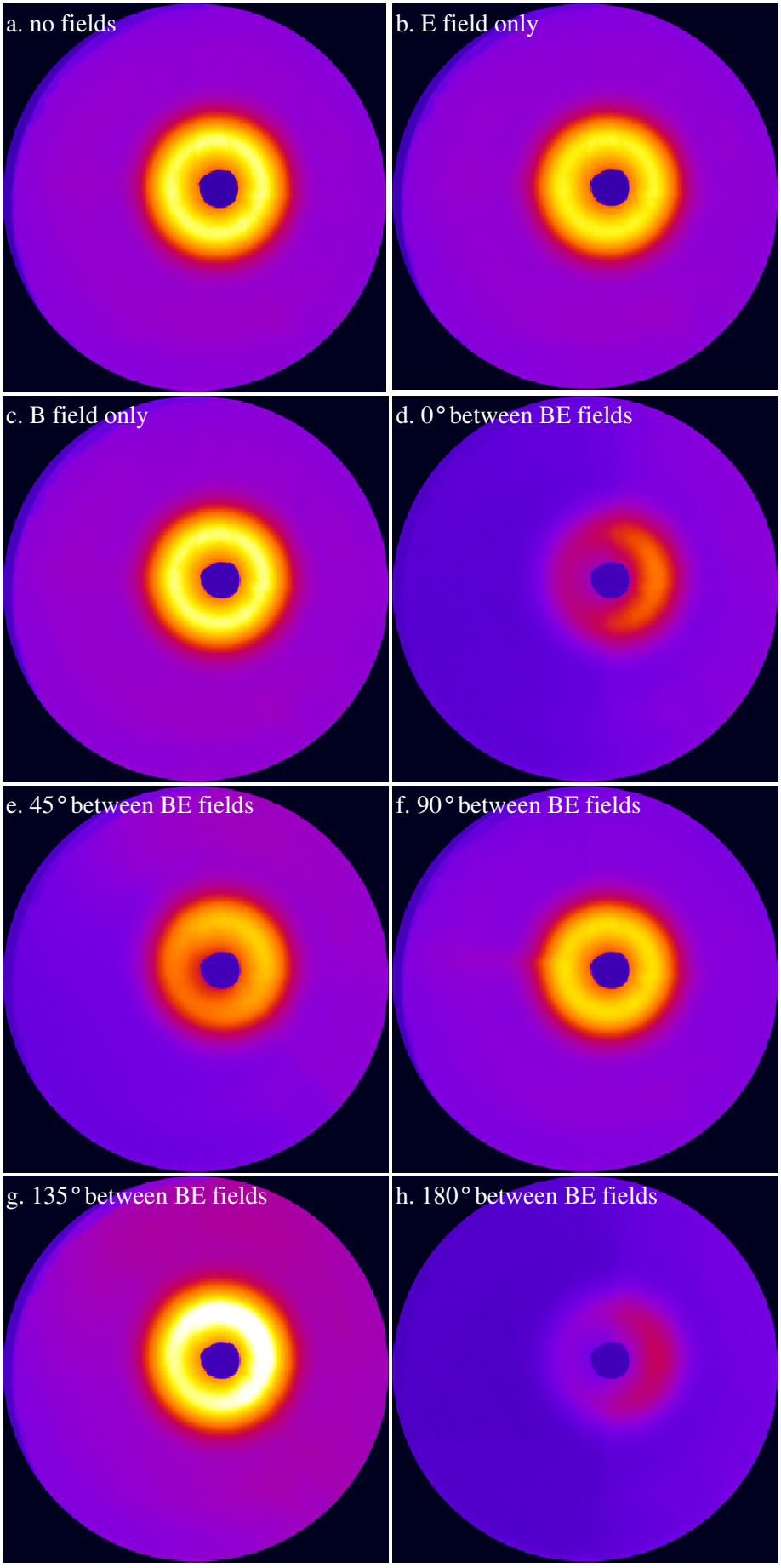

Figure 2. Scattering from 30% lysozyme in 30% glycerol solution under different combinations of electric and magnetic fields

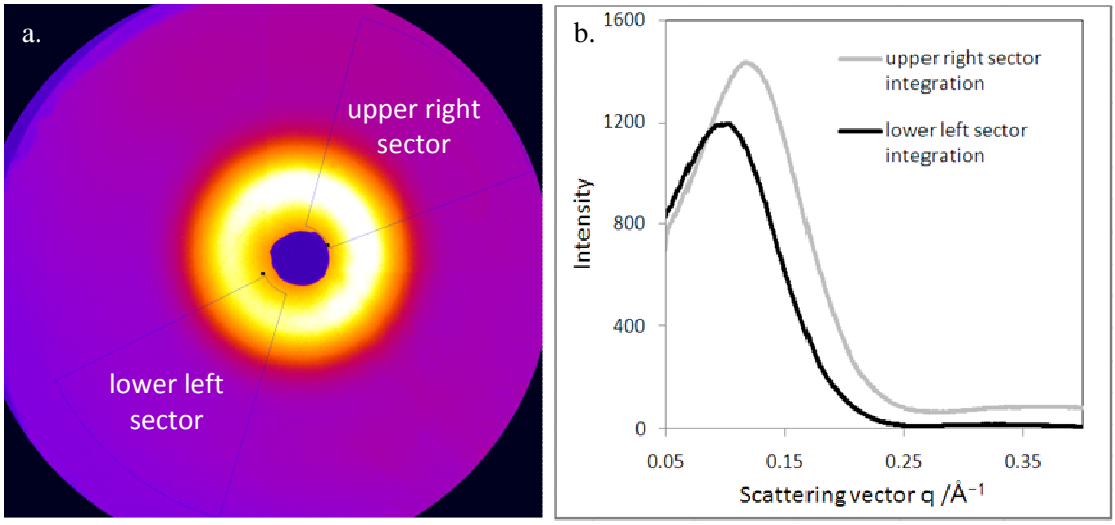

Figure 3. Sector integrations for the high and low intensity scattering from 30% lysozyme in 30% glycerol solution under simultaneous electric and magnetic fields with 135° between fields; a. sector areas, b. normalised integrations.

Appendix 1: Scattering from thin, uniaxially oriented rods on a pseudo-lattice.

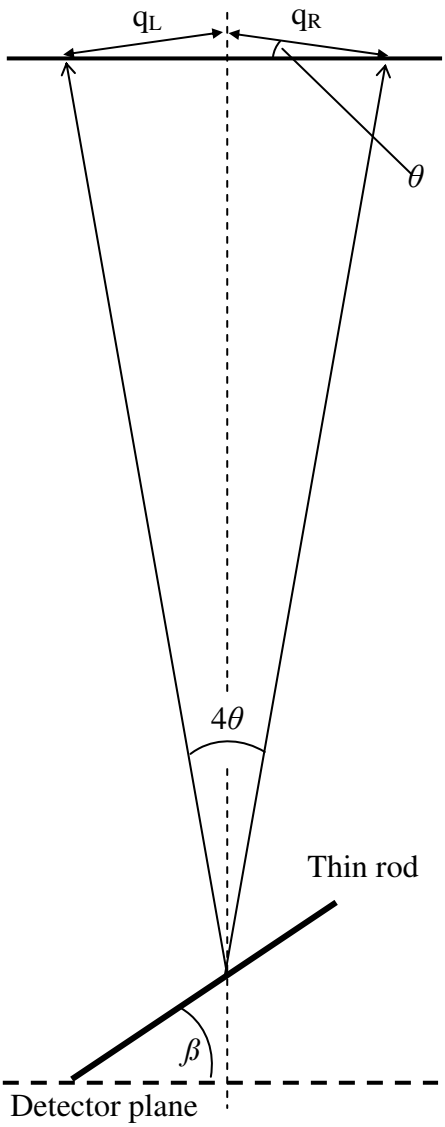

Figure 4: Geometry of scattering model

This hypothesis is based on scattering from highly oriented thin rods on a locally periodic, distorted pseudo-lattice. In 'real space', this is equivalent to a convolution of particles (uniaxially oriented rods) with the pseudo-lattice. Consequently, the scattering can be modelled as the product of a lattice function and particle function:

$$I(q) = I_0 . L(q) . P(q) \qquad (1)$$

where I_0 is a constant that depends on strength of the incident light, illuminated sample volume, detector response, acquisition time etc.

Fundamentally, the scattering from any homogeneous particle can be described by:

$$P(q) = I_0 . \left| \int_V \rho_e(\mathbf{r}) . \exp(-\mathbf{q}.\mathbf{r}) . d\mathbf{r} \right|^2 \qquad (2)$$

q.r is the vector 'dot product':

$$\mathbf{q}.\mathbf{r} = qr\cos\phi \qquad (3)$$

where q and r are the moduli (i.e. lengths) of the vectors and ϕ is the angle between the vectors.

For a very thin rod (i.e, thickness is negligible), of length L, Equation (2) becomes:

$$P(q) = I_0 \left| \rho_e . \int_{-L/2}^{L/2} \exp(-qr\cos\phi) . dr \right|^2 \qquad (4)$$

where ϕ is now the angle between the principal axis of the rod and the scattering vector **q**. This is shown in Figure 4.

It is important to note that **q** describes the change of direction from the vector describing incident light to that

describing the scattered light. Significantly, q is not perpendicular to the incident light and deviates from the plane of the detector by an angle of ± θ. Hence, $qr.\cos\phi$ may not be symmetrical about the incident vector.

If the orientation of the rod relative to the detector plane is described by the angle β, then:

$$\mathbf{q}_L.\mathbf{r} = qr\cos(\beta - \theta) \tag{5a}$$

$$\mathbf{q}_R.\mathbf{r} = qr\cos(\beta + \theta) \tag{5b}$$

The inherent symmetry of the cosine function means that these expressions are identical for β = 0° or 180°, and differ only in sign for ß = 90° or 270°, but they differ in magnitude for other values of β.

The integration in Equation 4 is given by Roe (ref. [1], p. 161):

$$P(q) = I_0\left(\frac{2}{qL\cos\phi}\right)^2.\sin^2\left(\frac{qL}{2}\cos\phi\right) \tag{6}$$

where $\phi = \beta \pm \theta$

The effect of the difference between Equations 5a and 5b is shown in Figure 5, for L = 20 nm and β = 80°. Clearly, the function decays much faster at low q, for the left-hand side (i.e. $\phi = \beta - \theta$).

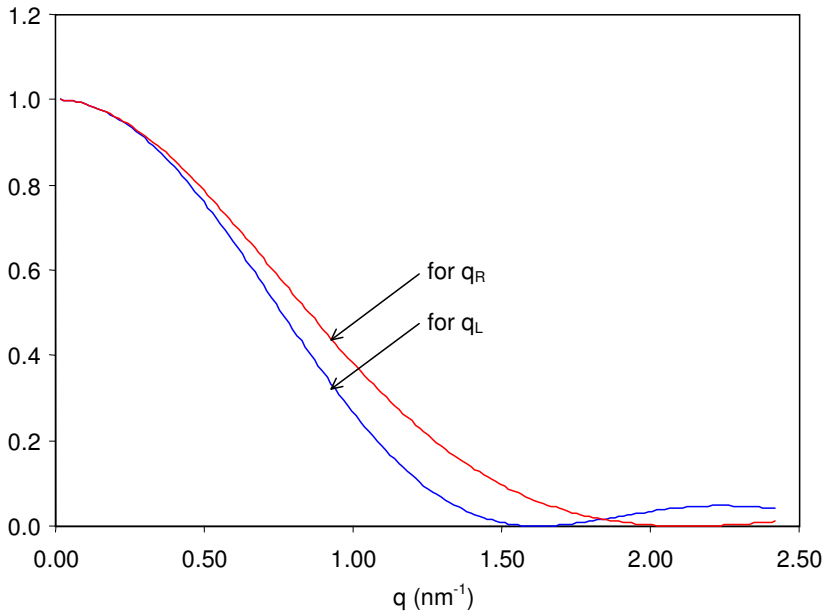

Figure 5: Left- and right-hand sides of P(q) for ß = 80°.

The pseudo-lattice can be modelled as a system where the distance between lattice points follows a Gaussian distribution about the mean d, (i.e. 'type 2' distortions (see [1]) with standard deviation σ:

$$L(q) = \frac{1 - A^2}{1 - 2A.\cos(qd) + A^2} \tag{7a}$$

where:

$$A = \exp\left(-\frac{q^2\sigma^2 d^2}{2}\right) \tag{7b}$$

The function L(q) is small at low q, rises to the main peak, then oscillates through one or more subsequent peaks, before settling down at a value of 1, at higher q. The peak position depends predominantly on d, although it is also affected by σ; the height and breadth also depend on σ. This is shown in Figure 6, for d = 10 nm and σ = 0.2.

The scattering is then modelled by Equation 1, where the maximum intensity depends on the lattice and particle functions. Significantly, this means that the differences in particle function on opposite sides of the pattern can produce different scattering maxima, as shown in Figure 7.

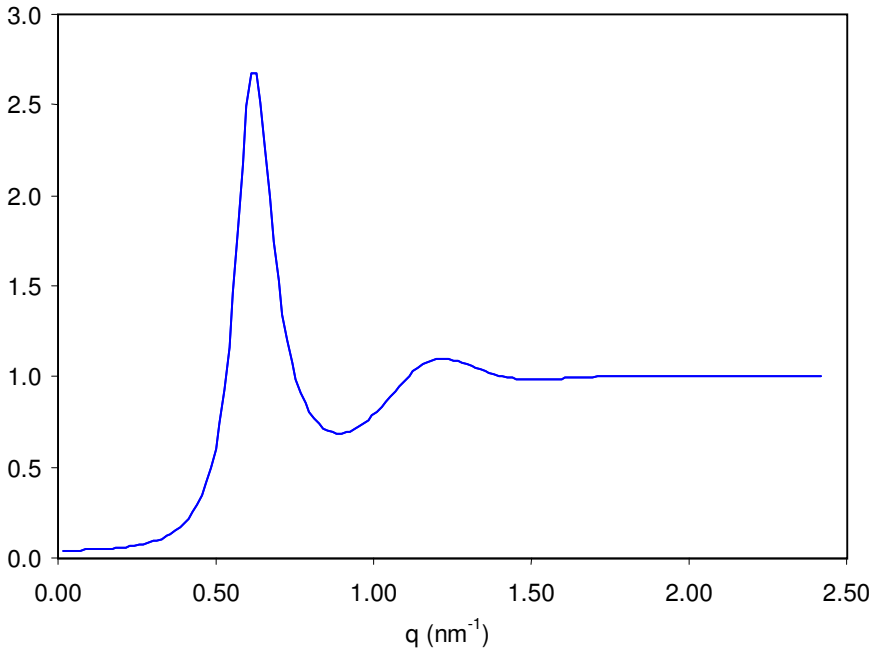

Figure 6: Lattice function, for d = 10 nm and σ = 0.2.

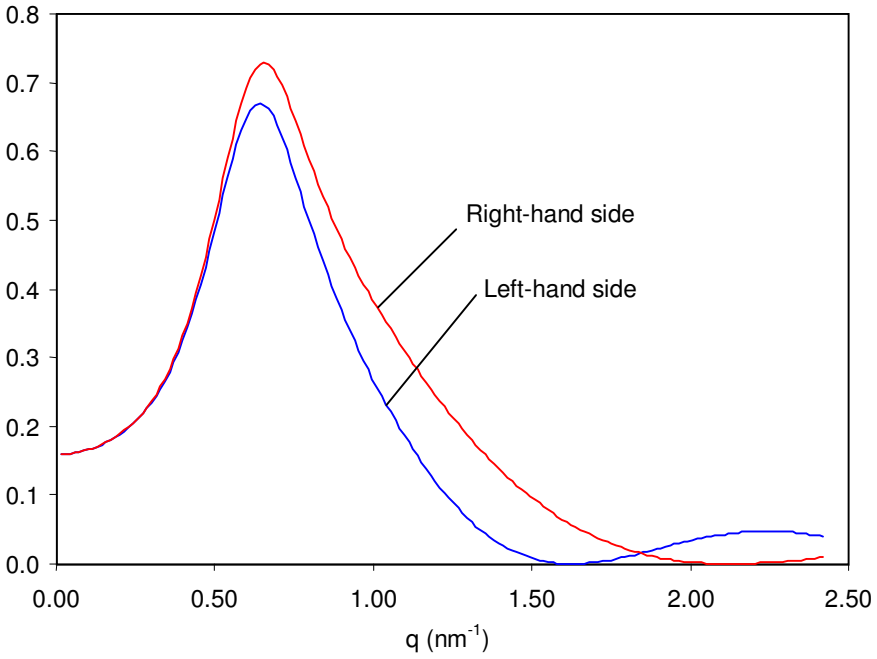

Figure 7: Modelled intensity, for L = 20 nm, d = 8 nm and σ = 0.4.

References

1. R-J. Roe, Methods of X-ray and Neutron Scattering in Polymer Science, Oxford University Press, New York, 2000.